Bioactive Materials 5 (2020) 309–317

Contents lists available at ScienceDirect

Bioactive Materials

journal homepage: http://www.keaipublishing.com/biomat

Colloidal forming of macroporous calcium pyrophosphate bioceramics in 3D-printed molds

Ya.Yu Filippov[a,b,*], E.D. Orlov[a], E.S. Klimashina[a,c], P.V. Evdokimov[a,c], T.V. Safronova[a,c], V.I. Putlayev[a,c], J.V. Rau[d]

[a] Department of Materials Science, Lomonosov Moscow State University, Moscow, Russia
[b] Institute of Mechanics Research, Lomonosov Moscow State University, Moscow, Russia
[c] Department of Chemistry, Lomonosov Moscow State University, Moscow, Russia
[d] Istituto di Struttura della Materia, Consiglio Nazionale delle Ricerche (ISM-CNR), Via del Fosso del Cavaliere 100, 00133, Rome, Italy

ARTICLE INFO

Keywords:
Bioceramics
Calcium pyrophosphate
Calcium metaphosphate
Colloidal forming
3D-printing
Kelvin structure

ABSTRACT

A technique for colloidal forming of $Ca_2P_2O_7$ macroporous bioceramics, based on low-pressure injection molding (LPIM) of a glycerol-water slip containing $Ca_2P_2O_7$ and $Ca(H_2PO_4)_2$ into a plastic mold fabricated via FDM 3D-printing, was proposed. Chemical reaction between the solid phases of the water containing slip - $Ca_2P_2O_7$ and $Ca(H_2PO_4)_2$, resulting in brushite ($CaHPO_4{\cdot}2H_2O$) formation, led to consolidation of the casting and preserved its complex architecture in the course of mold burning-out. Macroporous ceramics of Kelvin structure (70% macropores with the sizes from 2 up to 4 mm), based on a pre-defined composition with 10 wt% $Ca(PO_3)_2$ and sintered in liquid-phase regime, demonstrated a compressive strength of 1.4 ± 0.1 MPa at a density of 22 ± 2%. *In vitro* tests on bioactivity in SBF solution, as well as on resorption of the ceramics in model solution of citric acid, were carried out.

1. Introduction

Nowadays, resorbable ceramics have a great potential as a material for bone grafting substitute since it can guide and partially support bone ingrowth at the early stages of osteointegration, gradually dissolving and finally being replaced by bone *de novo* [1].

Among calcium phosphates, calcium pyrophosphate ($Ca_2P_2O_7$, CPP) is of particular interest for making bioresorbable bone implants, since it has potentially good resorbability [2–5]. At the same time, pathological deposition of calcium pyrophosphate dihydrate ($Ca_2P_2O_7{\cdot}2H_2O$, CPPD) in articular cartilage, meniscus, and intervertebral disc, known also as pyrophosphate arthropathy (or pseudogout disease), is the reason for a degenerative arthritis [6,7]. However, according to Lee et al. [8] and Lin et al. [9] CPP alone or with sodium pyrophosphate admixture do have certain potential as resorbable implant material and its presence should not cause the CPPD deposition. Discussing advantages of CPP, it should be noted that in the body environment at near physiological pH values CPP does not immediately transform into less soluble hydroxyapatite ($Ca_{10}(PO_4)_6(OH)_2$, HA) due to the extremely sluggish hydrolysis of the pyrophosphate anion according to the following reaction:

$$P_2O_7^{4-} + H_2O \rightarrow 2HPO_4^{2-}. \quad (1)$$

The hydrolysis obeys zero-order kinetics; temperature, pH, enzymes, cations (in particular, Mg^{2+}), concentration, ionic strength (in decreasing order of importance) affect the rate of the process. At human body temperature, in the pH range of 7–10, the typical hydrolysis time is *ca.* 10^3–10^5 h, this makes the contribution of reaction (1) insignificant in most cases [10–12]. However, in the presence of phosphatase-type enzymes, the hydrolysis to orthophosphate becomes possible in a shorter time [13], which can contribute to new bone formation.

Major challenge in fabrication of pyrophosphate ceramics relates to a low diffusion mobility of large pyrophosphate anions during sintering, assuming, therefore, significant temperature and duration of thermal treatment. These lead to a prevalence of recrystallization phenomena over densification; resulting ceramics have a low density and large grain size [5]. Such a problem can be partially solved by sintering in liquid-phase regime. The later requires an addition of a component that

Peer review under responsibility of KeAi Communications Co., Ltd.
* Corresponding author. Department of Materials Science, Lomonosov Moscow State University, Moscow, Russia.
E-mail addresses: filippovya@gmail.com (Y.Y. Filippov), orlovegor1712@yandex.ru (E.D. Orlov), alenakovaleva@gmail.com (E.S. Klimashina), pavel.evdokimov@gmail.com (P.V. Evdokimov), t3470641@yandex.ru (T.V. Safronova), valery.putlayev@gmail.com (V.I. Putlayev), giulietta.rau@ism.cnr.it (J.V. Rau).

https://doi.org/10.1016/j.bioactmat.2020.02.013
Received 23 October 2019; Received in revised form 18 February 2020; Accepted 19 February 2020

a b c

Fig. 1. a) Computer model of macroporous ceramic sample with the Kelvin structure, b) computer model of the mold for casting the sample, represented in (a), c) ABS-plastic mold made by the FDM 3D-printing.

ensures the formation of a liquid phase at a selected sintering temperature [14]. Low-melting calcium metaphosphate ($Ca(PO_3)_2$, CMP, melting point T_m = 990°C) can be used as such biocompatible additive, giving with CPP an eutectic at 970°C [15–17]. We have proposed CMP as a sintering additive to fabricate CPP ceramics elsewhere [18].

It is generally accepted that bone tissue regeneration occurs effectively when the implant has macro- and micropores providing circulation of interstitial fluid, vascularization and bone ingrowth (all treated within the term "osteoconductivity") [19]. Scaffolds manufactured by "conventional" techniques for making highly porous bodies such as foaming method, replication of polymer preforms or using sacrificial additive do not meet requirements on permeability (and, therefore, osteoconductivity) and strength properties for the macroporous implants. Therefore, the significance of macroporous ceramics with interconnected pores and high permeability is doubtless. Currently, the only technique for forming implants of given complex architecture and shape is rapid prototyping (more specifically, 3D-printing) [20–22].

Colloidal forming, which consists in casting of reactive slip under low pressure into a mold and subsequent consolidation of the slip due to a certain chemical reaction, is a promising technique to fabricate a green part of ceramics with a given complex shape and architecture. Bolarinwa et al. [2] fabricated CPP ceramics through the casting of brushite cement; the slip obtained by mixing of tricalcium phosphate with a solution of phosphoric and citric acids was casted into a mold, followed by heat treatment at temperatures of 400–1200 °C. In principle, this technique can be easily integrated into the flow-chart of rapid prototyping [22]. To the best our knowledge, no attempts to get osteoconductive CPP-ceramics via the technique of slip-casting into the mold fabricated by 3D-printing have been made so far. Gbureck et al. [23] used powder 3-D printing of tricalcium phosphate powder bonded with phosphoric acid followed by heat treatment to obtain composite ceramics based on tricalcium phosphate/calcium pyrophosphate with a given architecture. However, this type of printing has low lateral resolution inherent to this 3D-printing technique; low green density of as-printed model leads to insufficient sintering and, therefore, to low strength of the final ceramics. In the cited work [23], the authors had to fire ceramics at high temperature in order to reach tricalcium phosphate/CPP eutectic. It is reasonable to believe that in the case of slip casting under pressure into a mold, higher green density is attainable. Depending on quality of reproduction of the mold (it can be reproduced with a high precision from a computer model, *e.g.* by stereolithography 3D-printing), higher lateral resolution, better than 50 μm, can be also achieved.

Thus, the aim of this work is to elaborate osteoconductive bioresorbable ceramics based on calcium pyrophosphate with a given macroporous architecture by using colloidal forming of reactive slurry in special plastic mold made by the 3D-printing.

2. Materials and methods

2.1. Reagents and synthesis

CPP was prepared by thermal decomposition of brushite powder ($CaHPO_4{\cdot}2H_2O$), precipitated from a 1 M solutions of calcium nitrate $Ca(NO_3)_2{\cdot}4H_2O$ (Sigma Aldrich) and ammonium hydrophosphate $(NH_4)_2HPO_4$ (Sigma Aldrich); the product was then grinded in a planetary ball mill (Pulverisette, Fritsch, Germany) under acetone for 15 min. A powder mixture for making highly concentrated reactive slurry (slip) was prepared by ball milling of powders of CPP and monocalcium phosphate monohydrate $Ca(H_2PO_4)_2{\cdot}H_2O$ (Sigma Aldrich) under acetone for 15 min with mass ratio providing the following ratio of ceramics phases CPP/CMP = 90/10, 80/20 and 70/30.

2.2. Fabrication of macroporous and dense ceramics

The slip for casting was prepared by mixing the powder precursor of required composition with liquid (mixture of glycerol and distillated water) in a ratio powder/liquid of 2:1 by weight. The ratio of glycerol/distillated water in slip medium was established as 40/60 by volume. Thereafter, the slip was slowly casted into plastic mold with channels forming Kelvin structure [24] (Fig. 1a and b) under the pressure of 0.5 MPa. The castings were left at room temperature over a day at least. Such a technique can be regarded as a kind of low-pressure injection molding (LPIM). The use of a glycerol solution in water as dispersing medium allows 1) to improve ductility of the slurry, to increase its viscosity, avoiding phenomenon of press-filtration (rapid separation of solid phase from the slurry) during LPIM, and 2) to prevent too fast hardening of the slurry [25]. Plastic molds (Fig. 1 c) for casting an item with Kelvin structure (Fig. 1 a) were obtained from ABS-plastics using an FDM 3D-printer (Z Morph, Poland). Mold geometric parameters ensured the manufacture of castings with a diameter of 8 mm and various height up to 16 mm, with a fraction of interconnected macropores of 70%, maximum pore size of 4 mm, and beam thickness of 2 mm.

Thus obtained castings were thermally treated in a muffle furnace (Nabertherm, Germany; heating rate of 2 °C/min) to burn out gradually the plastics, not destroying casting geometry, and then sintered at 1000 °C for 1 and 3 h to form composite ceramics of desired structure. In the case of making dense model ceramics, the slip was casted into cylinder shape (diameter - 8 mm, height from 2 to 16 mm). The cylinders were subjected to heat treatment similar to the one described above.

2.3. Characterization

2.3.1. XRD analysis

X-Ray diffraction analysis (XRD) was conducted by the diffractometer with rotating anode Rigaku D/Max-2500 (Rigaku, Japan).

2.3.2. Microstructure investigation and electron probe microanalysis

Microstructure of the ceramics was studied by scanning electron microscopy (SEM) by a field-emission microscope LEO SUPRA 50VP (Carl Zeiss, Germany) in the secondary electron mode. To evaluate local chemical composition of the ceramics electron probe microanalysis (EDX-technique) was done with the help of INCA Energy300 (Oxford Instruments, UK) at 20 kV. Matrix correction was conducted using the XPP-ϕ(ρz) technique.

2.3.3. Mechanical properties

Compressive strength of the prepared ceramics was measured using cylindrical samples with diameter/height ratio of 1:2 (diameter - 8 mm, height - 16 mm). The samples were subjected to uniaxial compression by universal test machine P-05, equipped with multi-channel measuring system (Spider, Germany), along the cylinder axis at crosshead rate of 1 mm/min.

2.3.4. pH-measurements

To estimate dissolution kinetics of the ceramic granules of CPP and CMP with dimensions of 100–500 μm were prepared. Granules of CPP and CMP were prepared by crashing of samples of CPP sintering at 1000 °C during 1 h and samples of CMP after heat treatment at 300 °C for 6 h.

pH-measurements of water suspensions of the materials (CPP, CMP and their mixtures) were conducted. For this, 0.5 g of the ceramic granules of CPP, CMP or CPP/CMP were placed in 50 ml of distilled water and pH-measurements were carried with a dwell-time of 0.1 s and duration up to 24 h (Expert 001 pH-meter, Russia).

2.3.5. Assessment of bioactivity in vitro

Bioactivity of the samples was assessed by soaking the ceramics in 5SBF solution according to the procedure described in Ref. [26] at 37 °C for 24 and 120 h. Afterward, the surface of the ceramics was investigated by SEM. The rate of resorption (dissolution) of the ceramics as well as comparison with ceramics based on HA and TCP, were estimated from the experiments for pH-stating (at pH = 5) of ceramic granules (about 50 mg) with the sizes from 100 to 500 μm in solutions of 0.02 M citric acid (automatic titrator Titration Excellence T-50, Mettler-Toledo, Switzerland). Such a technique relates to the biomaterials resorption tests described in ISO 10993 [27], although, differing in some details. Yield of dissolution was estimated based on the amount of citric acid spent for the pH-stating for a certain period of time with respect to a consumption of acid for complete dissolution of the granules. Equilibrium solubility of HA, TCP and CPP phases and its variation with pH were calculated in water solutions at 25 °C using aquatic chemistry software MEDUSA/HYDRA [28].

3. Results and discussion

3.1. Phase formation upon hardening and thermal treatment of the castings

According to XRD, a small amount of brushite $CaHPO_4{\cdot}2H_2O$ was formed during hardening of the casted slip. Similar to curing of brushite cement, interlocked brushite crystals provided integrity of the castings and preserved their Kelvin macroporous when burning out plastic mold at the stage of thermal treatment. In addition to brushite, the phase of calcium dihydrogen pyrophosphate $CaH_2P_2O_7$ was also detected (Fig. 2). Such findings allow to wright the overall reaction leading to the consolidation of the casting as follows:

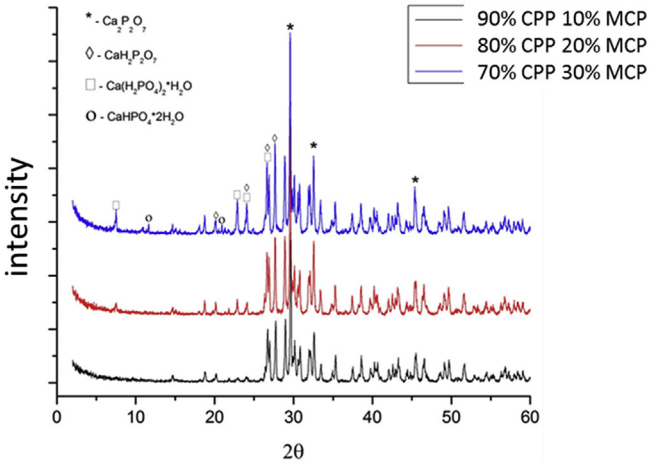

Fig. 2. XRD spectra of the hardened castings with different content of the starting reagents $Ca_2P_2O_7$ and $Ca(H_2PO_4)_2{\cdot}H_2O$, providing the ceramics with different ratio of CPP and CMP. The pointed ratio of ceramic phases is on the figure.

$$Ca_2P_2O_7 + Ca(H_2PO_4)_2{\cdot}H_2O + 3H_2O = 2CaHPO_4{\cdot}2H_2O + CaH_2P_2O_7. \quad (2)$$

One can see from equation (2) that water takes part in the reaction, *i.e.* the used slip has properties similar to a hydraulic cement of the brushite-type. The curing rate of the slip follows, in fact, pyrophosphate to orthophosphate conversion rate in the reaction (1), and depends on the amount of water in the slip (traces found in air-stored glycerol). For this reason, the curing time (at least, 1 h according to our estimation) significantly exceeds typical curing time of conventional brushite cement (being of the order of several minutes) [29]. This makes possible to conduct reliable casting by slow LPIM into the mold with rather complex geometry.

After heat treatment at 1000 °C for 1 h, the castings were transformed into composite ceramics consisting of CPP and CMP. Besides CPP from the starting batch, this phase also appeared during the thermolysis of brushite formed via the reaction (1), while the origin of CMP was the thermolysis of calcium dihydrogen pyrophosphate monohydrate:

$$2CaHPO_4{\cdot}2H_2O = Ca_2P_2O_7 + 5H_2O, \quad (3)$$

$$CaH_2P_2O_7 = Ca(PO_3)_2 + H_2O, \quad (4)$$

$$Ca(H_2PO_4)_2{\cdot}H_2O = Ca(PO_3)_2 + 3H_2O. \quad (5)$$

It should be noted that in the case of heat treatment for 3 h, the CMP phase was absent (Fig. 3); this can be explained by the decomposition of CMP to CPP and removal of phosphorus oxide in the form of a gaseous product at high temperature. EDX analysis of the above ceramics confirmed that Ca/P ratio decreased after 3 h heat treatment at 1000 °C (Fig. 4).

The statistical significance of the above results on composition of the ceramics was estimated using Student's independent two-sample *t*-test (equal variance, degree of freedom (*n*-1) was equal to 4). The values of *t* statistic between pairs of one- and 3-h sintered samples with the same CMP content were calculated and significance level *P* was found (Table 1).

Thus, we can conclude that the composition of the samples without calcium metaphosphate does not vary during sintering treatment, while in case of its presence an increase in the Ca/P ratio varies with a reliability of 90–99.9%, depending on composition. This confirms partial volatilization of CMP during sintering.

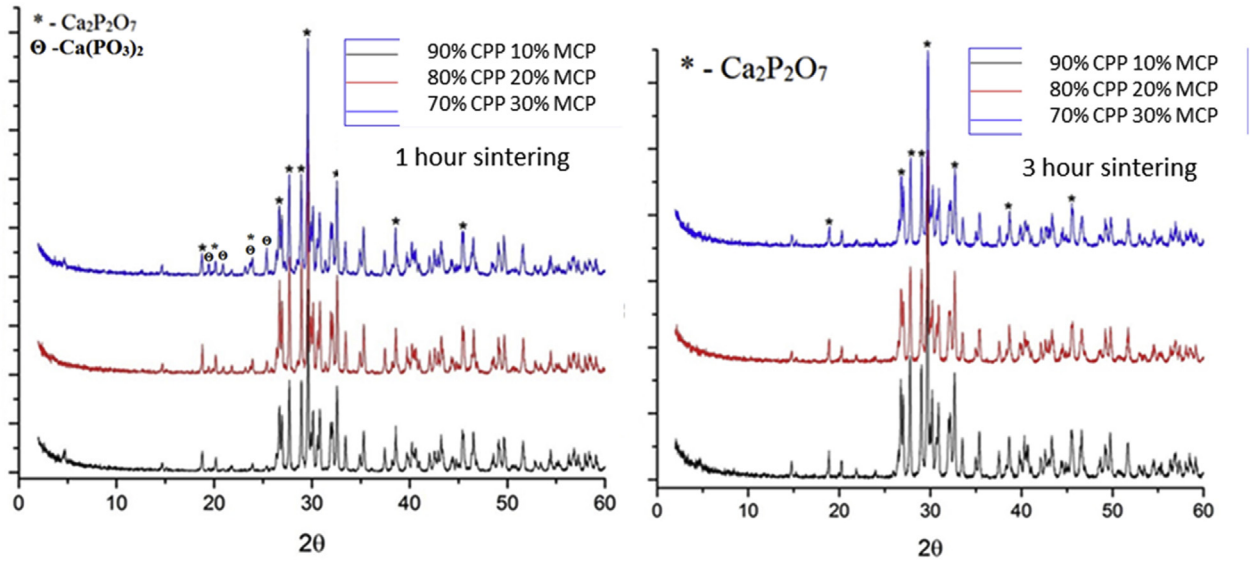

Fig. 3. XRD spectra of the ceramics with different CPP/CMP ratio sintered at 1000°C for 1 h (left) and 3 h (right).

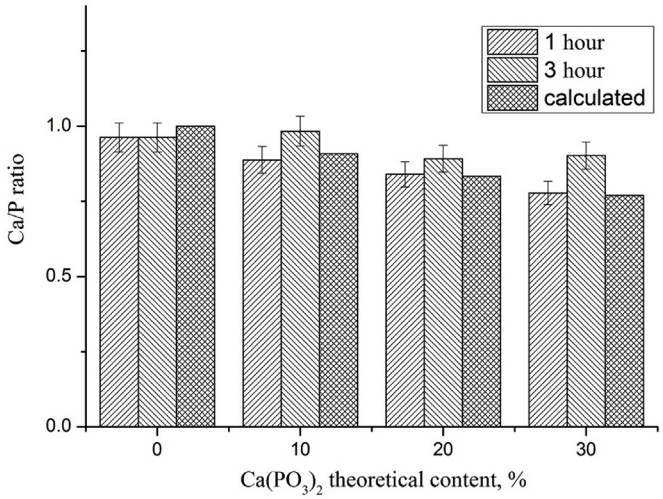

Fig. 4. Ca/P ratio (according to EDX analysis) of the ceramics with different CMP content sintered at 1000°C for 1 and 3 h; calculated values corresponding to overall stoichiometry of the raw mixtures are also given.

Table 1
Values of Student's *t* statistic and significance level (*P*) for the ceramics with different CMP content.

CMP content	0%	10%	20%	30%
t	0.13	2.93	1.84	4.72
P	No differences	0.99	0.9	0.999

3.2. Thermodynamics of CMP evaporation

In order to argue possibility of CMP evaporation, corresponding thermodynamic calculations were undertaken for the first time (to the best our knowledge) as it is described below. During sintering, the following reactions of CPP and CMP decomposition are possible, due to the evaporation of volatile phosphorus oxide P_4O_{10} (P_2O_5) (sublimation at T_{sub} = 360°C, boiling point T_b = 865°C for an aqueous azeotrope with 92.4% P_2O_5 [12,30]):

$$4Ca(PO_3)_{2\ (s)} \rightarrow 2Ca_2P_2O_{7(s)} + P_4O_{10(g)}, \quad (6)$$

$$4Ca(PO_3)_{2\ (l)} \rightarrow 2Ca_2P_2O_{7(s)} + P_4O_{10(g)}, \quad (6')$$

$$6Ca_2P_2O_{7(s)} \rightarrow 4Ca_3(PO_4)_{2(s)} + P_4O_{10(g)}. \quad (7)$$

To evaluate the occurrence of the reactions (6, 7) on the thermodynamic basis, the following equations related to the temperature dependence of the Gibbs energy of formation of the substances involved in the reactions (6, 7) were used: $\Delta_fG^\circ_T(Ca_2P_2O_7) = -3475.9 + 1.5441T - 0.1051TlnT$ (± 11) kJ/mol, $\Delta_fG^\circ_T(Ca(PO_3)_2) = -3334.8 + 6.1561T - 0.695TlnT$ (± 12) kJ/mol [31], $\Delta_fG^\circ_T$ ($Ca_3(PO_4)_2$) = - 4200.1 + 0.912T [32]; for gaseous phosphorus oxide, the value of $\Delta_fG^\circ_{1273}(P_4O_{10}(g)) = -2048.16$ kJ/mol was obtained using the data from Refs. [33–38]. For the reaction (6), the decomposition of CMP into CPP, $\Delta_rG^\circ_{1273}(7) \approx 156$ kJ/mol CMP, and for the reaction (7), decomposition of CPP into TCP and gaseous phosphorus oxide, $\Delta_rG^\circ_{1273}$ (8) ≈ 298 kJ/mol CPP. Estimation of the equilibrium partial pressure of the P_4O_{10} vapor according to the formula $\Delta_rG^\circ_T$ (7, 8) = - $RT\cdot\ln p(P_4O_{10(g)})$, leads, in the first case to $p(P_4O_{10(g)})$ (6) ≈ $4\cdot10^{-2}$ Pa, and in the second, to $p(P_4O_{10(g)})$ (7) ≈ $6\cdot10^{-8}$ Pa. Therefore, the driving force of the reaction (6), as well as of the reaction (6′), is substantially higher compared to the one of (7). The studies of incongruent evaporation of calcium phosphates in vacuum by mass-spectrometry methods [36] gave evidence for the following processes:

$$Ca_3(PO_4)_{2(s)} \rightarrow 3CaO_{(s)} + 2PO_{2(g)} + 0.5O_{2(g)}, \quad (8)$$

$$Ca_2P_2O_{7(s)} \rightarrow Ca_3(PO_4)_{2(s)} + 2PO_{2(g)} + 0.5O_{2(g)}, \quad (9)$$

$$Ca(PO_3)_{2(s)} \rightarrow Ca_2P_2O_{7(s)} + 0.5P_4O_{10(g)}, \quad (10)$$

$$Ca(PO_3)_{2(l)} \rightarrow Ca_2P_2O_{7(s)} + 0.5P_4O_{10(g)}. \quad (10')$$

The dissociation pressure decreases in the following order $Ca(PO_3)_2$ > $Ca_2P_2O_7$ > $Ca_3(PO_4)_2$: for solid CMP, it is *ca.* $6\cdot10^{-2}$ Pa at 900 °C, and the pressure of phosphorus oxide over liquid CMP at 1000 °C corresponds to *ca.* 0.6 Pa [39]. Recalculation of the data on the dissociation pressure vs temperature [40] gives $\Delta_rG^\circ_{1273}$ (6) = 126.4 kJ (124.6 kJ for the reaction (6')) and $\Delta_rG^\circ_{1273}$(9) = 496.6 kJ. The above estimations suggest that the incongruent evaporation of CPP occurs in a less extent compared to CMP.

It should be noted that in a wet atmosphere, the incongruent evaporation might be different: phosphoric acids can act as a volatile phosphorus compound, *i.e.* in fact, pyrohydrolysis (hydrolytic decomposition due to a reaction with water vapor) of calcium phosphate occurs. The version of pyrohydrolysis reaction of CMP into CPP and phosphoric acid (T_b = 158°C [12,30]) is presented below:

$$2Ca(PO_3)_{2(s)} + 3H_2O_{(g)} \rightarrow Ca_2P_2O_{7(s)} + 2H_3PO_{4(g)} \quad (11)$$

To estimate roughly the value of $\Delta_f G^\circ_T(H_3PO_{4(g)})$, the Trouton's rule, claiming $\Delta S^\circ_b = \Delta H^\circ_b/T_b \approx 88$ J/(mol·K), was used. This rule is applicable for weakly associated liquids, indeed, the proton solvent with a network of hydrogen bonds is not the case. Nevertheless, to understand the possibility of occurrence of the pyrohydrolytic reaction of the type (12), such an approximation looks reasonable. Then, taking $\Delta_f H^\circ_{298}(H_3PO_{4(g)}) = \Delta_f H^\circ_{298}(H_3PO_{4(g)}) + \Delta H^\circ_b$ and $\Delta_f S^\circ_{298}(H_3PO_{4(g)}) = S^\circ_{298}(H_3PO_{4(g)}) + \Delta S^\circ_b - 3/2 S^\circ_{298}(H_{2(g)}) - S^\circ_{298}(P_{white(s)}) - 2S^\circ_{298}(O_{2(g)})$, neglecting the specific heat, one can find that $\Delta_f G^\circ_{1273}(H_3PO_{4(g)}) \approx -1534$ kJ/mol; then $\Delta_r G^\circ_{1273}$ (11) ≈ - 41 kJ. The Gibbs energy of the reaction (11) was estimated under non-standard conditions (partial pressure of water vapor is less than 1 atm) using the formula [40] $\Delta_r G_T = \Delta_r G^\circ_T + R\mathrm{Tln}(p/p_0)$, where p is the partial pressure of water vapor and p_0 is an atmospheric pressure. Then, taking into account that at a humidity of 60% under laboratory conditions $p \approx 2$ kPa, one can get $\Delta_r G_{1273}$ (11) ≈ 0.7 kJ. A negative or close to zero Gibbs energy indicates that the equilibrium (11) is rather shifted to the right, toward the evaporation of volatile phosphorus compounds. Under real condition of sintering, when the humidity of sintering environment ranges from 0 to 60%, the pattern of incongruent evaporation is situated between border cases described by equations (6) and (11). The Gibbs free energy of the incongruent evaporation is, then, in the range -201 kJ $< \Delta_r G_T < 0.7$ kJ, and the dissociation pressure is $1\ 4{\cdot}10^{-2}$ Pa $< p < 2{\cdot}10^3$ Pa; the vapor phase is composed of phosphorus oxide (V) and its decomposition products (PO_2, O_2), and phosphoric acids - orthophosphoric and polyphosphoric ones. The presence of a gas flow carrying away the volatile decomposition products is an additional factor contributing to a complete reaction.

3.3. Microstructure and density of the ceramics

In Fig. 5, the microstructure of model ceramic cylinders with initially different contents of CMP sintered at 1000 °C for 1 h and 3 h is shown. Increase in the sintering time leads to a significant grain growth, however, the ceramics still contain a significant amount of isolated pores. For the samples with CPP/CMP = 90/10 and 80/20 sintered for 1 h, the difference in grain sizes is not noticeable, however, in the case of the composition 70/30, large grains are can be observed.

Densification of the ceramics proceeds rather slowly, in contrast to recrystallization: for instance, density of the ceramics with the compositions 90/10 and 80/20 does not undergo noticeable changes after 3 h of sintering; by the end of this time interval, differences in the density of the materials of different initial compositions are leveled out (Table 2). The interplay between the densification and grain growth of the prepared ceramics can be ruled out based on their phase composition and microstructure features. CMP enhances liquid-phase sintering due to the formation of the melt, rearranging the particles of the powder and facilitating recrystallization of CPP through its dissolution - precipitation. As sintering proceeds, the above-described incongruent evaporation of CPP occurs, accompanied by crystallization and an increase in the grain size and coarsening of the remaining pores. After the melt disappears, the removal of the closed pores under the conditions of the solid-phase sintering becomes extremely difficult due to low mobility of pyrophosphate anion. This situation corresponds to a lower pore mobility compared to the mobility of grain boundaries, i.e. the prevalence of recrystallization processes over densification, being typical for CPP ceramics sintering [11]. Thus, the reasons for appearance of large (up to 20 μm) pores are: 1) evaporation of the CMP-enriched melt (and/or crystallization upon subsequent cooling), and 2) further coarsening of the remaining pores under solid-phase sintering. On the one hand, an increase in the amount of the initial CMP evaporating upon sintering leads to a “spongy” material, and, on the other hand, the presence of large amount of the liquid phase contributes to a more efficient sintering. If duration of sintering does not exceed 1 h, then the first process prevails, whereas sintering for 3 h gives evidence of intensive grain growth. Large, well-faceted grains are quite noticeable in the area occupied by transgranular cracking on the fracture surface of the ceramics, this area increases with increase in sintering time from 1 to 3 h, and increase in the initial fraction of CMP from 10 to 30 wt% (Fig. 5).

Table 2
Relative density of the model ceramic samples sintered at 1000 °C for 1 and 3 h.

Sintering time, h	90% CPP/10% CMP	80% CPP/20% CMP	70% CPP/30% CMP
1	86	80	77
3	83	82	83

relative density values (± 2%).

3.4. Mechanical properties

Strength values of the model cylinder ceramics correlate well with the microstructure observations and the data on ceramic density (Fig. 6). The statistical significance of the difference in compressive strength of the ceramics was estimated using Student's independent two-sample t-test (equal variance, degree of freedom (n-1) was equal to 4). The values of t statistic between pairs of materials with different

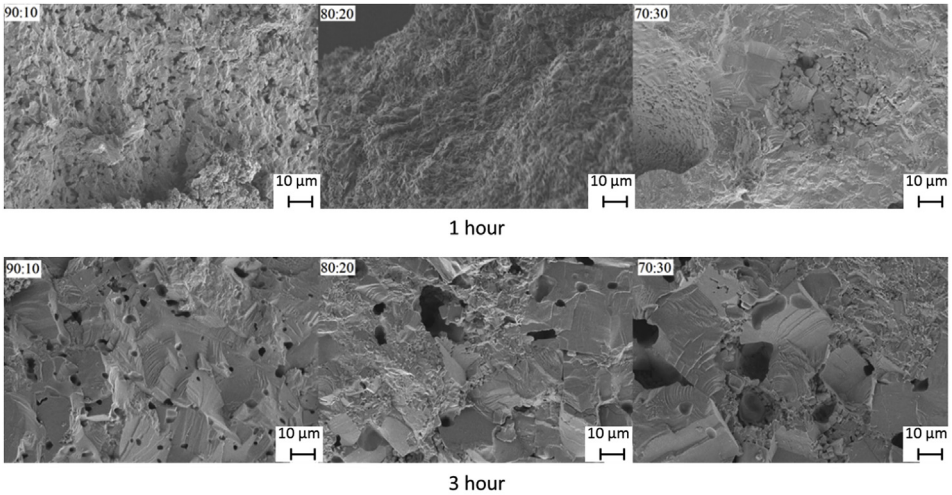

Fig. 5. SEM images of the fracture surface of the ceramic samples with different initial content of CMP sintered at 1000 °C for 1 h (top) and 3 h (bottom).

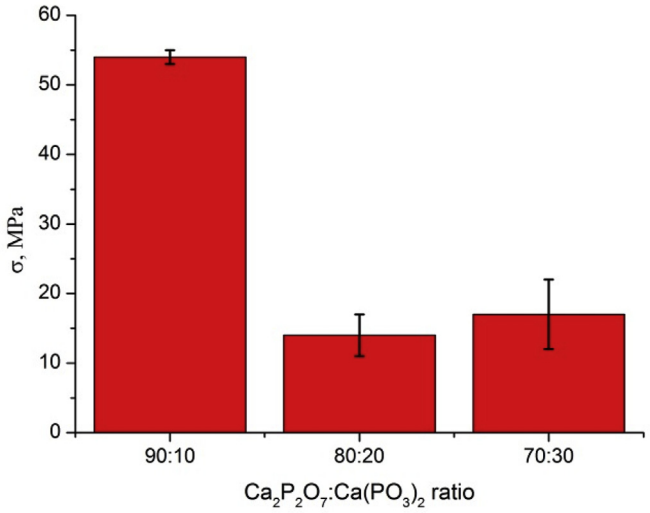

Fig. 6. Compressive strength of model ceramic cylinders with different contents of CMP sintered at 1000 °C for 1 h.

Table 3
Values of Student's *t* statistic and significance level (*P*) for pairwise selections of ceramics with different CMP content.

CMP content	10% and 20%	10% and 30%	20% and 30%
t	45.2	33.36	2.36
P	> 0.999	> 0.999	0.975

CMP content were calculated and significance level *P* was found (Table 3).

One can conclude that compressive strength of the ceramics with 10 and 20% as well as 10 and 30% CPP has significantly different values with a reliability more than 99.9%. In the case of the pair of 20 and 30% CMP difference in compressive strength is at the level of about 97.5%.

The highest compressive strength (54 ± 1 MPa) was observed in the case of the ceramics with a density of 86% obtained by sintering at 1000 °C for 1 h with an estimated content of CMP of 10 wt%. Earlier, we reported on compressive strength of CPP-ceramics up to 25 MPa [14], being significantly lower the above value of 54 MPa. Unfortunately, other strength data are hardly available from the literature, making difficult comparison. Thus, this composition and sintering conditions were used to fabricate macroporous ceramics with the Kelvin architecture by the LPIM in the ABS-plastic mold, as described in the Materials and Methods section (Fig. 7). Density of the obtained

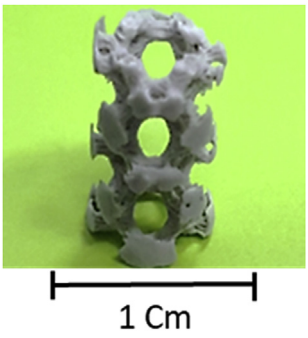

Fig. 7. Macroporous ceramic sample with Kelvin architecture (initial composition 90 wt% CPP/10 wt% CMP) fabricated by colloidal forming into a 3D-printed ABS mold, followed by plastics burning out and sintering at 1000 °C for 1 h.

macroporous ceramics was of 22 ± 2%, since 70% of density was lost due to the macropores introduced with the 3D-printed mold. Therefore, 27 ± 7% of the pores were located in the scaffold, such a porosity corresponds to that observed in microstructure images (Fig. 5). The strength of the macroporous item was 1.4 ± 0.1 MPa, which seems to be enough to perform the simplest manipulations when applied (gripping with hands and tools, grinding to size, *etc.*). Such strength characteristics of macroporous sample are in qualitative agreement with the Gibson-Ashby model [41] for deformation of open-cell structures. According to this model, brittle fracture of an open-cell sample occurs when the elastic limit σ_{el} related to the beam bending is reached: $\sigma_{el} \sim 0.03 \cdot E_k \ (1-\varphi)^2(1+(1-\varphi)^{1/2})^2$, where the φ is fraction of macropores, E_k is the elastic modulus of the frame. If one puts $E_k = 0.78E$ (assuming that E - Young's module for dense CPP ceramics, is less than 1 GPa), then for $\varphi = 0.7$, $\sigma_{el} < 4$ MPa, which is rather close to the experimental strength value.

For further testing, model and macroporous ceramic samples sintered for 1 h were selected due to their fine-grained microstructure structure, being important not only for strength, but also for relevant biological properties.

3.5. Evaluation of the ceramics bioactivity

To evaluate bioactivity of the materials in vitro, experiments on soaking of the ceramic samples in 5SBF solution at 37 °C for various times were performed. High numbers of nuclei of HA deposited on the surface were observed after 24 h, and a uniform layer of tangled HA crystals covering the entire surface of the materials was observed after 120 h of soaking, being indicative of potentially high bioactivity of the samples (Fig. 8).

It should be noted that widely used ISO 23317:2014(en) standard to access materials bioactivity [42], referred to Kokubo and Takadama [43], deals with conventional non-concentrated SBF. In this work, we used five-time supersaturated SBF solution [26], which allows to evaluate bioactivity more quickly. In any case, validity of such techniques (related both to SBF and to more concentrated solutions, and aimed at assessment of apatite forming ability) should be confirmed by *in vivo* experiments (see, *e.g.* criticism of the technique by Bohner and Lemaiˆtre [44]).

Titration experiments were conducted with ceramic granules from 100 to 500 μm in size, prepared by crushing macroporous and model samples and sieving fragments through the appropriate sieves, in pH-stating mode (at pH = 5) by continuous addition of 0.02 M citric acid to simulate the ceramics resorption. The value of pH = 5 was chosen based on the following considerations: 1) dissolution at pH less than 5 is too fast and does not allow to notice a difference between the samples under study, while at pH more than 5 (*e.g.*, at pH = 7) the dissolution rate is very slow, prolonging the experiment from several hours to several days, 2) osteoclasts in bone resorption lacunae create approximately the same value of pH [45]. Bearing in mind the change in the predominant forms of calcium during titration with citric acid, as it comes from the calculations of ionic equilibria, the equations for the dissolution of the ceramic samples can be described as:

$$Ca_3(PO_4)_{2(s)} + 2C_6H_8O_{7(solution)} \rightarrow 2CaC_6H_6O_{7(solution)} + Ca(H_2PO_4)_{2(solution)}, \quad (12)$$

$$Ca_2P_2O_{7(s)} + C_6H_8O_{7(solution)} \rightarrow CaC_6H_6O_{7(solution)} + CaH_2P_2O_{7(solution)}. \quad (13)$$

The amount of acid necessary to keep the pH-value fixed was used to calculate the degree of dissolution of the samples (Fig. 9a). Calculated equilibrium solubility of TCP and CPP vs pH is plotted in Fig. 9b. It is noteworthy that at pH > 5.5–6 (the position of the crossover of HA, TCP- and CPP-curves, marked by circle in Fig. 9b, depends on the accuracy in determining constants of ion equilibria), CPP is more soluble than TCP, in accordance with solubility products values K_S of

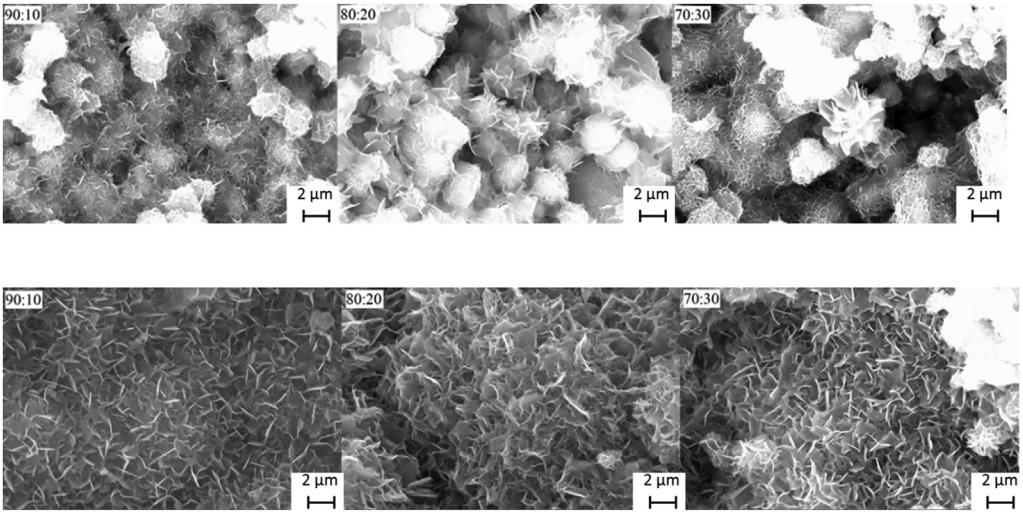

Fig. 8. SEM images of the surface of the ceramic materials with different contents of CMP, incubated in 5SBF solution for 24 h (top) and 120 h (bottom) at 37 °C.

these phases ($pK_S(Ca_2P_2O_7)$ = 14.7, $pK_S(Ca_3(PO_4)_2)$ = 28.92 [25]). However, at lower pH-values, the situation is reversed due to the pronounced dependence of TCP solubility on pH. This is caused by the fact that pyrophosphoric acid is stronger than orthophosphoric one (*e.g.*, at the third stage of dissociation $pK_{a3}(HPO_4^{2-})$ = 12.35; $pK_{a3}(H_2P_2O_7^{2-})$ = 6.65 [46]), and therefore, the PO_4^{3-}-anion is protonated to a greater extent, providing an increase in the solubility in acidic region. With this regard, experimental curves of solubility of the ceramic granules at pH = 5 (*i.e.* left to the crossover point discussed above, Fig. 9 a) are arranged in expected manner, when the worst-case solubility (resorption) is demonstrated by CPP ceramic sample. However, at pH > 5 (for example, at pH = 7.4 (blood plasma)), the CPP ceramics will be the most soluble sample. This feature of CPP material is important from the viewpoint of better "passive" resorption of the implant, *i.e.* the resorption in the absence of osteoclasts. It should be noted that the trace amounts of unevaporated CMP presented in the ceramics do not change the established pH-trend of CPP solubility, since metaphosphates have even weaker pH-dependence of solubility, due to the fact that polyphosphoric acids are stronger than pyrophosphoric one.

Based on the above considerations, it is clear why the pH of samples sintered for three or more hours is neutral, in contrast with the samples with a sintering time of 1 h. CPP rather slowly turns into HA, but CMP, as a polyphosphate with longer chain and, therefore, less stable, hydrolyzes to orthophosphate much faster [10]. As final products of hydrolysis (14), the most stable in aqueous solution HA and phosphoric acid are formed:

$$10Ca(PO_3)_2 + 7H_2O = Ca_{10}(PO_4)_6(OH)_2 + 4H_3PO_4. \quad (14)$$

According to equation (6), a decrease in pH occurs due to the release of phosphoric acid. Thus, the pH decrease of the solution in contact with the prepared ceramics can be considered as an indicator of the presence of CMP in the sample. At the very beginning of sintering, the CMP acts as a sintering agent with respect to the CPP powder, gradually decomposing with the release of volatile phosphorus compounds, thus avoiding acidification of the surrounding solution. Review of Vasant and Joshi [47] as well as reported preclinical trials [8,48] allow to conclude that bioceramics based on CPP are rather promising, although, neither evaluation of resorbability nor degradation behavior were reported so far.

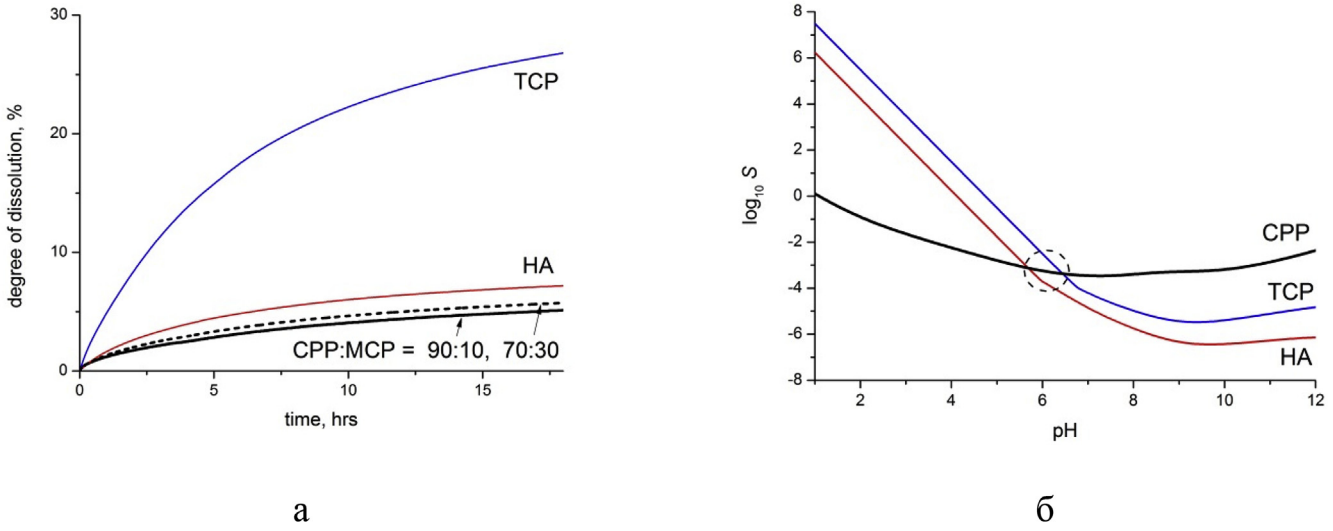

Fig. 9. a) Dissolution kinetics of the ceramic granules CPP:MCP = 90:10 and 70:30 at pH = 5; for comparison, the behavior of HA-granules (HA-curve) and TCP-granules (TCP-curve) are shown, b) calculated profiles of logarithm of equilibrium solubility of CPP (at $[P_2O_7^{4-}]$ = 0.5 mM), and TCP, HA (at $[PO_4^{3-}]$ = 1 mM) vs pH.

4. Conclusions

A new method of colloidal forming of $Ca_2P_2O_7$ macroporous bioceramics, based on low-pressure injection molding (LPIM) of a glycerol-water slip containing $Ca_2P_2O_7$ and $Ca(H_2PO_4)_2{\cdot}H_2O$ into a plastic mold fabricated via the FDM 3D-printing, was proposed. Chemical reaction between the solid phases of the slip - $Ca_2P_2O_7$ and $Ca(H_2PO_4)_2{\cdot}H_2O$, resulting in brushite, led to consolidation of the casting and preserved its complex architecture in the course of mold burning-out.

Calcium metaphosphate formed from $Ca(H_2PO_4)_2{\cdot}H_2O$ and $CaH_2P_2O_7$ during heat treatment of preceramic item facilitates liquid-phase sintering of the ceramics above 970 °C. In the course of sintering, incongruent evaporation of the calcium-metaphosphate-enriched melt occurs. Substantial release of $Ca(PO_3)_2$ is beneficial for avoiding low pH of water solutions contacting with the ceramics, affecting the density and microstructure of the ceramics. The maximum relative density (86 ± 2%) and compressive strength (54 ± 1 MPa) were observed for the ceramics of pre-defined composition with 10 wt% $Ca(PO_3)_2$, sintered at 1000 °C for 1 h. Macroporous ceramics of Kelvin structure (70% macropores with the sizes from 2 up to 4 mm), based on the same composition and sintered under similar conditions, demonstrated a compressive strength of 1.4 ± 0.1 MPa at a density of 22 ± 2%.

In vitro bioactivity test results evidence the formation on the materials surface of the HA nuclei after 24 h and of the HA layer after 120 h of soaking. Simulation of resorption of the ceramics by dissolving in citric acid solution at pH = 5 showed that the rate of resorption of the obtained pyrophosphate ceramics is lower than for ceramics made of tricalcium phosphate (*ca.* in a factor of 5) and even of hydroxyapatite (*ca.* in a factor of 1.6). Such a behavior of $Ca_2P_2O_7$ was associated with weaker protonation of pyrophosphate anion during dissolution of the ceramics.

Finally, the prepared ceramic materials are promising for potential use on osteoplastics.

Declaration of competing interest

The authors declare that they have no known competing financial interests or personal relationships that could have appeared to influence the work reported in this paper.

Acknowledgements

This study was partially supported by the RFBR (grants No. 18-33-00789 mol_a, 18-08-01473, 19-03-00940). Equipment purchased using the funding of Development Program of Moscow State University was used.

References

[1] M. Bohner, Resorbable biomaterials as bone graft substitutes, Mater. Today 13 (1–2) (2010) 24–30, https://doi.org/10.1016/S1369-7021(10)70014-6.
[2] A. Bolarinwa, U. Gbureck, P. Purnell, M. Bold, L.M. Grover, Cement casting of calcium pyrophosphate based bioceramics, Adv. Appl. Ceram. 109 (5) (2010) 291–295, https://doi.org/10.1179/174367609X459586.
[3] T.V. Safronova, V.I. Putlyaev, A.V. Knot'ko, V.K. Krut'ko, O.N. Musskaya, S.A. Ulasevich, N.A. Vorob'eva, V.D. Telitsin, Calcium phosphate ceramic in the system $Ca(PO_3)_2$–$Ca_2P_2O_7$ based on powder mixtures containing calcium hydrophosphate, Glass Ceram. 75 (7–8) (2018) 279–286, https://doi.org/10.1007/s10717-018-0072-z.
[4] T.V. Safronova, V.I. Putlyaev, K.A. Bessonov, V.K. Ivanov, Ceramics based on calcium pyrophosphate nanopowders, Process. Appl. Ceram. 7 (1) (2013) 9–14, https://doi.org/10.2298/PAC1301009S.
[5] T.V. Safronova, A.V. Kuznetsov, S.A. Korneychuk, V.I. Putlyaev, M.A. Shekhirev, Calcium phosphate powders synthesized from solutions with $[Ca^{2+}]/[PO_4^{3-}] = 1$ for bioresorbable ceramics, Cent. Eur. J. Chem. 7 (2) (2009) 184–191, https://doi.org/10.2478/s11532-009-0016-0.
[6] Pritzker KPH Crystal-associated arthropathies: what's new in old joints? J. Am. Geriatr. Soc. 28 (1980) 439–445, https://doi.org/10.1111/j.1532-5415.1980.tb01116.x.
[7] Mitrovic DR Pathology of articular deposition of calcium salts and their relationship to osteoarthrosis, Ann. Rheum. Dis. 42 (1983) 19–23, https://doi.org/10.1136/ard.42.suppl_1.19.
[8] J.H. Lee, B.S. Chang, U.O. Jeung, K.W. Park, M.S. Kim, C.K. Lee, The first clinical trial of beta-calcium pyrophosphate as a novel bone graft extender in instrumented posterolateral lumbar fusion, Clin. Orthopedic Surg. 3 (3) (2011) 238–244, https://doi.org/10.1007/s00776-011-0047-1.
[9] F.H. Lin, C.C. Lin, H.C. Lu, C.M. Liu, J.S. Sun, C.Y. Wang, Mechanical properties and histological evaluation of sintered β-$Ca_2P_2O_7$ with $Na_4P_2O_7{\cdot}10H_2O$ addition, Biomaterials 16 (1995) 793–802, https://doi.org/10.1016/0142-9612(95)99642-Y.
[10] YuF. Zhdanov, Chemistry and Technology of Polyphosphates, Khimiya, Moscow, 1979.
[11] J. Green, Reversion of molecularly dehydrated sodium phosphates, Ind. Eng. Chem. 42 (8) (1950) 1542, https://doi.org/10.1021/ie50488a025.
[12] J.R. Van Wazer, Phosphorus and its compounds, Chemistry 1 (1958).
[13] A.S. Spirin, Molecular Biology: Ribosome Structure and Protein Biosynthesis, (1986).
[14] T.V. Safronova, V.I. Putlayev, YaYu Filippov, D.S. Larionov, P.V. Evdokimov, A.E. Averina, E.S. Klimashina, V.K. Ivanov, Porous ceramics based on calium pyrophosphate, New Refractories 1 (2015) 46–51, https://doi.org/10.1007/s11148-015-9818-0.
[15] M.N. Safina, T.V. Safronova, E.S. Lukin, Calcium phosphate based ceramic with a resorbable phase and low sintering temperature, Glass Ceram. 64 (7–8) (2007) 238–243, https://doi.org/10.1007/s10717-007-0060-1.
[16] W.L. Hill, G.T. Faust, D.S. Reynolds, System CaO–P_2O_5, Am. J. Sci. 242 (9) (1944) 457–477.
[17] G. Troemel, H.I. Harkcort, W. Hotop, Z. Anorg, Untersuchungen im System CaO-P_2O_5-SiO_2, Inside Chem. 256 (5–6) (1948) 253–272, https://doi.org/10.1002/zaac.19482560501.
[18] T.V. Safronova, T.B. Shatalova, YaYu Filippov, V.K. Krutko, O.N. Musskaya, A.S. Safronov, O.U. Toshev, Ceramics based on Ca2P2O7 — Ca(PO3)2 system obtained by sintering samples from hardening mixtures based on calcium citrate and monocalcium phosphate monohydrate//Materials, Science 9 (2019) 31–40, https://doi.org/10.31044/1684-579X-2019-0-9-31-40.
[19] S.M. Barinov, V.S. Komlev, Approaches to the fabrication of calcium phosphate-based porous materials for bone tissue regeneration, Inorg. Mater. 52 (4) (2016) 383–391, https://doi.org/10.1134/S0020168516040026.
[20] F. Baino, E. Fiume, J. Barberi, S. Kargozar, J. Marchi, J. Massera, E. Verne, Processing methods for making porous bioactive glass-based scaffolds – a state-of-the-art review, Int. J. Appl. Ceram. Technol. 16 (2019) 1762–1796, https://doi.org/10.1111/ijac.13195.
[21] V.M. Ievlev, V.I. Putlyaev, T.V. Safronova, P.V. Evdokimov, Additive technologies for making highly permeable inorganic materials with tailored morphological architectonics for medicine, Inorg. Mater. 51 (13) (2015) 1295–1313, https://doi.org/10.1134/S0020168515130038.
[22] W.M. Sigmund, N.S. Bell, L. Bergstorm, Novel powder-processing methods for advanced ceramics, J. Am. Ceram. Soc. 83 (7) (2000) 1557–1574, https://doi.org/10.1111/j.1151-2916.2000.tb01432.x.
[23] U. Gbureck, T. Hölzel, I. Biermann, J.E. Barralet, L.M. Grover, Preparation of tricalcium phosphate/calcium pyrophosphate structures via rapid prototyping//, J. Mater. Sci. Mater. Med. 19 (4) (2008) 1559–1563, https://doi.org/10.1007/s10856-008-3373-x.
[24] Lord Kelvin (Sir William Thomson) LXIII, On the division of space with minimum partitional area, Philos. Mag. Ser. 5 (151) (1887) 503–514, https://doi.org/10.1080/14786448708628135 24.
[25] YaYu Filippov, A.A. Vlasikhina, E.S. Klimashina, P.V. Evdokimov, V.I. Putlayev, Creation of three-dimensional ceramic structures with prescribed architecture based on the system $Ca_2P_2O_7$–$CaNa_2P_2O_7$, Glass Ceram. 75 (11–12) (2019) 446–450, https://doi.org/10.1007/s10717-019-00109-2.
[26] F. Barrere, C.A. van Blitterswijk, K. de Groot, P. Layrolle, Influence of ionic strength and carbonate on the Ca-P coating formation from SBFx5 solution, Biomaterials 23 (2002) 1921, https://doi.org/10.1016/S0142-9612(01)00318-0.
[27] Biological Evaluation of Medical Devices. Part 14: Identification and Quantification of Degradation Products from Ceramics, (2009) ISO 10993-14.
[28] (a) I. Puigdomenech, MEDUSA: make equilibrium diagrams using sophisticated algorithms, www.kemi.se/medusa, (2009);
(b) see also, G. Eriksson, An algorithm for the computation of aqueous multicomponent, multiphase equilibria, Anal. Chim. Acta 112 (1979), https://doi.org/10.1016/S0003-2670(01)85035-2 375-3834.
[29] M. Bohner, H.P. Merkle, V.P. Landuyt, G. Trophardy, J. Lemaiˆtre, Effect of several additives and their admixtures on the physico-chemical properties of a calcium phosphate cement, J. Mater. Sci. Mater. Med. 1 (2000) 111–116, https://doi.org/10.1023/A:1008997118576.
[30] Ullmann's Enciklopedia of Industrial Chemistry, Phosphoric Acids and Phosphates, Wiley-VCH Verlag GmbH & Co. KGaA, 2002, pp. 679–722.
[31] M.H. Sandström, D. Boström, E. Rosen, Determination of standard Gibbs free energy of formation for $Ca_2P_2O_7$ and $Ca(PO_3)_2$ from solid-state EMF measurements using yttria stabilised zirconia as solid electrolyte, J. Chem. Thermodyn. 38 (2006) 1371–1376, https://doi.org/10.1016/j.jct.2006.01.018.
[32] E. Yamasue, K. Shimizu, K. Nagata, Direct determination of standard Gibbs energies of the formation of $4CaO{\cdot}P_2O_5$ and $3CaO{\cdot}P_2O_5$ by transpiration method, ISIJ Int. 53 (10) (2013) 1828–1835, https://doi.org/10.2355/tetsutohagane.101.169.
[33] L.V. Gurvich, I.V. Veitz, et al., Thermodynamic Properties of Individual Substances, fourth ed. in 5 volumes, Hemisphere Pub Co., NY, L, 1989, p. 1.
[34] L.V. Gurvich, V.S. Yungman, et al., Thermodynamic properties of the components of Combustion's products, in: V.P. Glushko (Ed.), 3 Volumes, USSR Ac. of Sci, M., 1956.
[35] JANAF Thermochemical Tables, The Dow Chemical Company Mitland, Michigan,

1965.
[36] V.P. Glushko (Ed.), Thermal Constants of Substances, 1965-1968, pp. 1–3.
[37] D.D. Wagman, et al., US NBS Technical Note, 207 (1965—1969), pp. 1–4.
[38] E.K. Kazenas, Thermodynamics of Evaporation of Double Oxides, Science, Moscow, 2004, p. 551.
[39] I.A. Rat'kovskiy, B.A. Butilin, G.I. Novikov, Mass-spectroscopy study of evaporation of potassium, calcium and aluminium metaphosphates, Inorg. Mater. 10 (1975) 76 (in Russ).
[40] G.B. Naumov, B.N. Ryzhenko, I.L. Khodakovsky, Handbook of Thermodynamic Data, (1971).
[41] L.J. Gibson, M.F. Ashby, Cellular Solids: Structure and Properties, Cambridge University Press, 1999, https://doi.org/10.1017/CBO9781139878326.
[42] ISO 23317:2014(en)Implants for surgery — in vitro evaluation for apatite-forming ability of implant materials, https://www.iso.org/obp/ui/#iso:std:iso:23317:ed-3:v1:en.
[43] T. Kokubo, H. Takadama, How useful is SBF in predicting in vivo bone bioactivity? Biomaterials 27 (2006) 2907–2915, https://doi.org/10.1016/j.biomaterials.2006.01.017.
[44] M. Bohner, J. Lemaitre, Can bioactivity be tested in vitro with SBF solution? Biomaterials 30 (2009) 2175–2179, https://doi.org/10.1016/j.biomaterials.2009.01.008.
[45] R. Baron, L. Neff, D. Louvard, P.J. Courtoy, Cell-mediated extracellular acidification and bone resorption: evidence for a low ph in resorbing lacunae and Localization of a 100-Kd Lysosomal membrane protein at the osteoclast ruffled border, J. Cell Biol. 101 (6) (1985) 2210–2222, https://doi.org/10.1083/jcb.101.6.2210.
[46] W. Stumm, J.J. Morgan, Aquatic Chemistry, third ed., John Wiley & Sons, New York, 1996.
[47] Sonal R. Vasant, M.J. Joshi, A review on calcium pyrophosphate and other related phosphate nano bio-materials and their applications, Rev. Adv. Mater. Sci. 48 (2017) 44–57, https://doi.org/10.1186/s40824-018-0149-3.
[48] K.S. Lee, H.S. Han, Y.C. Kim, J.H. Lo Han, H. Seung R, H.S. Lee, J.S. Chang, D.H. Lee, Evaluation of porous b-calcium pyrophosphate as bioresorbable bone graft substitute material, Mater. Res. Innovat. 19 (2) (2015) 86–90, https://doi.org/10.1179/1433075X14Y.0000000215.